Elastic reflection of low-energy electrons from polycrystalline gold targets

1998 J. Phys. D: Appl. Phys. 31 36

(http://iopscience.iop.org/0022-3727/31/1/006)

J. Phys. D: Appl. Phys. **31** (1998) 36–42. Printed in the UK PII: S0022-3727(98)83405-0

Elastic reflection of low-energy electrons from polycrystalline gold targets

C M Kwei†, Y F Chen‡ and C J Tung§

† Department of Electronics Engineering, National Chiao Tung University, Hsinchu, Taiwan
‡ Precision Instrument Development Centre, Science-Based Industrial Park, Hsinchu, Taiwan
§ Department of Nuclear Science, National Tsing Hua University, Hsinchu, Taiwan

Received 14 April 1997

Abstract. Monte Carlo calculations to study the influence of solid-state, polarization, exchange and relativistic effects on the angular distribution and the reflection coefficient for electrons elastically reflected from gold surfaces have been performed. Elastic differential cross sections were determined using relativistic Dirac equations with a solid-atom potential including the polarization and exchange effects. Inelastic differential inverse mean free paths were computed using the extended Drude dielectric function for volume and surface excitations. These showed that the polarization effect made a contribution to elastic differential cross sections at small scattering angles, whereas, the exchange and relativistic effects contributed to these cross sections at large scattering angles. These effects are important to the angular distribution and the elastic reflection coefficient for electron energies below 400 eV. Monte Carlo results calculated in this work are in very good agreement with experimental data.

1. Introduction

Many applications in modern surface physics require one to study the interaction of electrons with solids. Among these applications, elastic scattering of electrons plays an important role in the interpretation of experimental data [1–8] measured by scanning electron microscopy (SEM), electron probe microanalysis (EPMA), Auger electron spectroscopy (AES) and so on. Furthermore, much attention has been paid to elastically reflected electrons because these have a number of advantages over inelastic ones [9–17]. First of all, the contrast in SEM images is larger for elastically reflected electrons, by more than an order of magnitude, than it is for inelastically reflected electrons [18]. Moreover, better resolution and smaller depth profiles can be obtained in SEM images for elastically reflected electrons. Another important advantage is that the greater dependence of elastically reflected electrons on the atomic number may be used to study the surface of alloys [19].

Monte Carlo (MC) simulations have frequently been applied to study the transport of electrons in solids. In recent years, such simulations have been performed to determine the angular distribution of elastically reflected electrons [20–23]. Free-atom scattering potentials such as the Thomas–Fermi–Dirac (TFD) potential [24] and the Hartree–Fock (HF) potential were employed in the calculation of elastic differential cross sections. Polarization and exchange effects were both neglected in the derivation of these cross sections. Since atoms in solids are bound to the media, elastic differential cross sections should be computed using the Hartree–Fock–Wigner–Seitz (HFWS) solid-atom potential [25]. In this potential, the polyhedral cell surrounding the atom is replaced by a Wigner–Seitz sphere within which the nuclear field is completely screened. Thus, elastic differential cross sections at small scattering angles are reduced by the solid-state effect. Furthermore, it has been found that the exchange effect was quite important for elastic scattering of electrons, especially those of low energies, in solids. The polarization effect also played a role for low-energy electrons at small scattering angles. The solid-state, polarization and exchange effects are all included in the present work.

Previously, we have employed elastic differential cross sections calculated using the non-relativistic model to study the characteristics of electrons elastically reflected from solids with low and intermediate atomic numbers. For solids of high atomic numbers, these cross sections are less accurate than those derived using the relativistic model. In this work, we determined elastic differential cross sections by solving relativistic Dirac equations for

0022-3727/98/010036+07$19.50

a potential considering the polarization and the exchange effects. This potential was constructed by calculating a HFWS electron density distribution for solid atoms with the ionic polarizability obtained from optical data. Electron inelastic mean free paths (IMFP) for volume and surface excitations were determined by the dielectric theory using an extended Drude function [26–28]. Applying the above cross section data to MC simulations showed that the angular distribution and the reflection coefficient of electrons elastically backscattered from gold surfaces were in good agreement with experimental data. These results showed also that the exchange effect was significant for electron energies below about 400 eV.

2. Theory

2.1. Elastic scattering

Dirac equations describing elastic scattering of an electron with total energy, W, from a spherically symmetrical potential, $V(r)$, are expressed by [29]

$$\frac{\mathrm{d}P_l^{\pm}(r)}{\mathrm{d}r} + \frac{\kappa_{\pm}P_l^{\pm}(r)}{r} + \frac{(W - V(r) + c^2)}{c}Q_l^{\pm}(r) = 0 \quad (1)$$

$$\frac{\mathrm{d}Q_l^{\pm}(r)}{\mathrm{d}r} + \frac{\kappa_{\pm}Q_l^{\pm}(r)}{r} - \frac{(W - V(r) - c^2)}{c}P_l^{\pm}(r) = 0 \quad (2)$$

where

$$\kappa_+ = -l - 1 \qquad \text{for } l = 0, 1, 2\ldots \quad (3)$$

$$\kappa_- = l \qquad \text{for } l = 1, 2, 3\ldots \quad (4)$$

and $P_l^{\pm}$ and $Q_l^{\pm}$ are the radial parts of the partial-wave-expanded Dirac equations. The plus and minus signs correspond to spin up and spin down respectively. Note that atomic units (au) are used throughout this work unless otherwise specified. By eliminating $Q_l^{\pm}(r)$ and substituting

$$P_l^{\pm}(r) = \eta^{1/2}G_l^{\pm}(r) \quad (5)$$

in equations (1) and (2), where

$$\eta = (W - V + c^2)/c \quad (6)$$

one transforms the radial Dirac equations into the Schrödinger-like wave equations

$$\frac{\mathrm{d}^2G_l^{\pm}(r)}{\mathrm{d}r^2} + \left(K^2 - U_{\pm}(r) - \frac{l(l+1)}{r^2}\right)G_l^{\pm}(r) = 0 \quad (7)$$

where

$$U_{\pm}(r) = \frac{2WV - V^2}{c^2} - \frac{\kappa_{\pm}}{r\eta}\frac{\mathrm{d}\eta}{\mathrm{d}r} + \frac{3}{4}\left(\frac{1}{\eta}\frac{\mathrm{d}\eta}{\mathrm{d}r}\right)^2 - \frac{1}{2\eta}\frac{\mathrm{d}^2\eta}{\mathrm{d}r^2} \quad (8)$$

and $K = (W^2 - c^4)^{1/2}/c$ is the wavenumber of the electron. Equation (7) may be solved under the initial condition

$$G_l^{\pm}(r) \underset{r\to 0}{\longrightarrow} r^{l+1} \quad (9)$$

and the asymptotic condition

$$G_l^{\pm}(r) \underset{r\to\infty}{\longrightarrow} r[j_l(Kr) \mp \tan\delta_l^{\pm} n_l(Kr)] \quad (10)$$

where j_l and n_l are spherical Bessel functions and $\delta_l^{\pm}$ are the lth scattering phase shifts.

To account for the polarization and the exchange effects, we let the scattering potential be a sum of several terms,

$$V(r) = V_S(r) + V_e(r) + V_p(r) \quad (11)$$

where $V_S(r)$ is the static potential, $V_e(r)$ is the exchange potential and $V_p(r)$ is the polarization potential. The static scattering potential is given by

$$V_S(r) = \begin{cases} -\dfrac{Z}{r} + \dfrac{1}{r}\displaystyle\int_0^r 4\pi r'^2\rho(r')\,\mathrm{d}r \\ \quad + \displaystyle\int_r^{R_{WS}} 4\pi r'\rho(r')\,\mathrm{d}r' & \text{for } r \le R_{WS} \\ 0 & \text{for } r > R_{WS} \end{cases} \quad (12)$$

where Z is the atomic number, $\rho(r)$ is the HFWS electron density distribution and R_{WS} is the Wigner–Seitz radius, all associated with the solid atom. The exchange effect may be dealt with by the Mittleman–Watson (MW) potential [30]. In this case, the wavenumber, K, of the electron is replaced by the local momentum, $K_L(r)$, as suggested by Riley and Truhlar [31]:

$$V_e(r) = -\frac{1}{\pi K_L(r)}\left(K_L(r)P(r) - \frac{1}{2}(K_L^2(r) - P^2(r)) \times \ln\left|\frac{K_L(r) + P(r)}{K_L(r) - P(r)}\right|\right). \quad (13)$$

In equation (13) the local Fermi momentum, $P(r)$, is related to the electron density, $\rho(r)$, of an unperturbed atom in the following manner:

$$P(r) = (3\pi^2\rho(r))^{1/3} \quad (14)$$

and

$$K_L(r) = (K^2 + P^2(r))^{1/2}. \quad (15)$$

Considering the polarization of an atom in the field of a scattered electron, we apply the Buckingham-type polarization potential [32–35]

$$V_p(r) = -\frac{\alpha_{ion}r^2}{2(r^2 + r_c^2)^3} \quad (16)$$

where α_{ion} is the ionic polarizability of the unperturbed atom and r_c is the cut-off parameter related to the size of the atom. Previously, we have derived the ionic polarizability for a free atom without considering the solid-state effect. Here we adopt a procedure proposed by Rehr *et al* [36] to extract this ionic polarizability from experimental optical data containing the solid-state effect. The cut-off parameter in equation (16) is set to R_{WS} as suggested by Joshipura and Mohanan [34].

For calculations of the phase shifts, we may divide r into two regions separated by r_0 where $V(r_0)$ is negligible in comparison with K^2. The solution of equation (7) in the region $r > r_0$ is given by equation (10), whereas we use the finite-difference method to solve this equation in the

region $r \le r_0$. Derivatives of the radial wavefunction are given by

$$\left.\frac{\mathrm{d}^2 G_l^{\pm}}{\mathrm{d}r^2}\right|_{r=r_i} = \frac{2}{r_{i+1}-r_{i-1}}\left(\frac{G_l^{\pm}(r_{i+1})-G_l^{\pm}(r_i)}{r_{i+1}-r_i} - \frac{G_l^{\pm}(r_i)-G_l^{\pm}(r_{i-1})}{r_i - r_{i-1}}\right) \tag{17}$$

where $i = 1, 2, 3, \ldots$ is the interval number of radius, r, in the finite-difference method. On substituting equation (17) into equation (7), we obtain

$$G_l^{\pm}(r_{i+1}) = G_l^{\pm}(r_i) + (r_{i+1}-r_i)\left[\frac{G_l^{\pm}(r_i)-G_l^{\pm}(r_{i-1})}{r_i - r_{i-1}} - \frac{r_{i+1}-r_{i-1}}{2}\left((K^2 - U_{\pm}(r_i)) - \frac{l(l+1)}{r_i^2}\right)G_l^{\pm}(r_i)\right]. \tag{18}$$

An iteration may be applied to equation (18) from a point near the nucleus up to r_0. The phase shifts, $\delta_l^{\pm}$, may be obtained by applying the boundary condition that $\mathrm{d}G_l^{\pm}/\mathrm{d}r$ are continuous at $r = r_0$.

The elastic scattering cross section of an unpolarized electron in the solid is given by [37]

$$\frac{\mathrm{d}\sigma}{\mathrm{d}\Omega} = |f(\theta)|^2 + |g(\theta)|^2 \tag{19}$$

where

$$f(\theta) = \frac{1}{2\mathrm{i}K}\sum_{l=0}^{\infty}\{(l+1)[\exp(2\mathrm{i}\delta_l^+) - 1] + l[\exp(2\mathrm{i}\delta_l^-) - 1]\}P_l(\cos\theta) \tag{20}$$

$$g(\theta) = \frac{1}{2\mathrm{i}K}\sum_{l=1}^{\infty}[\exp(2\mathrm{i}\delta_l^-) - \exp(2\mathrm{i}\delta_l^+)]P_l^1(\cos\theta) \tag{21}$$

θ is the polar scattering angle and $P_l(\cos\theta)$ and $P_l^1(\cos\theta)$ are the Legendre and the associated first-order Legendre polynomials respectively.

2.2. Inelastic interaction

Inelastic interactions between an incident electron and the solid consist mainly of volume and surface excitations. Volume excitations, contributed by electrons deep inside the solid, may be described by the IMFP, whereas surface excitations, arising from electrons near the surface, may be characterized by the surface excitation probability (SEP).

According to the dielectric theory, the IMFP, λ_i, for an electron of energy E in a homogeneous and isotropic solid is given by [38, 39]

$$\lambda_i^{-1}(E) = \frac{1}{\pi E}\int_0^E \mathrm{d}\omega \int_{q_-}^{q_+}\frac{\mathrm{d}q}{q}\,\mathrm{Im}\left(-\frac{1}{\varepsilon(q,\omega)}\right) \tag{22}$$

where $\varepsilon(q,\omega)$ is the complex dielectric function in terms of the momentum transfer, q, and the energy transfer, ω, Im( ) is the imaginary part of the negative inverse dielectric function and $q_{\pm} = (2E)^{1/2} \pm [2(E-\omega)]^{1/2}$ are derived from the conservation of energy and momentum.

Similarly, the SEP, representing the mean number of surface excitations by an electron across a solid surface, can also be treated by the dielectric theory. Under the condition of a negligible recoil effect, Ritchie [40] and Raether [26] have, respectively, derived the SEP for normally and obliquely incident electrons. Considering the recoil effect, we have derived the SEP for an electron of energy E with incident angle α with respect to the surface normal. The SEP is given by [41]

$$P_{\mathrm{S}}(\alpha, E) = P_{\mathrm{S}^+}(\alpha, E) + P_{\mathrm{S}_-}(\alpha, E) \tag{23}$$

where

$$P_{\mathrm{S}\pm}(\alpha, E) = \frac{2}{\pi E(\cos\alpha)} \times \int_0^E \mathrm{d}\omega \int_{q_-}^{q_+}\mathrm{d}q\,\frac{|q_s'|}{q^3}\,\mathrm{Im}\left(\frac{(\varepsilon-1)^2}{\varepsilon(\varepsilon+1)}\right) \tag{24}$$

$$q_s' = \left[q^2 - \left(\frac{\omega + (q^2/2)}{(2E)^{1/2}}\right)^2\right]^{1/2}\cos\alpha \pm \left(\frac{\omega + (q^2/2)}{(2E)^{1/2}}\right)\sin\alpha. \tag{25}$$

Since q_s' is different for positive and negative signs in equation (25), there is an asymmetrical effect in the SEP with respect to scattering angle orientations. This effect has been confirmed experimentally [42–44]. The probability of n surface excitations by an electron crossing the solid surface obeys Poisson statistics [39, 45–48], namely

$$P_n = \frac{1}{n!}[P_s(\alpha, E)]^n \exp[-P_s(\alpha, E)]. \tag{26}$$

Therefore, the probability of an electron crossing the solid surface without exciting any surface plasmon is proportional to $\exp[-P_s(\alpha, E)]$.

The model dielectric function used in this work is identical to that used previously. Here we present a brief synopsis. The real and imaginary parts of the dielectric function are given by [26, 28]

$$\varepsilon_1(q,\omega) = \varepsilon_b - \sum_i \frac{A_i[\omega^2 - (\omega_i + q^2/2)^2]}{[\omega^2 - (\omega_i + q^2/2)^2]^2 + (\omega\gamma_i)^2} \tag{27}$$

$$\varepsilon_2(q,\omega) = \sum_i \frac{A_i\gamma_i\omega}{[\omega^2 - (\omega_i + q^2/2)^2]^2 + (\omega\gamma_i)^2} \tag{28}$$

where A_i, γ_i and ω_i are, respectively, the oscillator strength, damping coefficient and critical-point energy associated with the ith interband transition. Note that we include in equation (27) a background dielectric constant, ε_b, due to the influence of polarizable ion cores [49]. Values of parameters in equations (27) and (28) may be determined by fitting equation (28), in the limit $q \to 0$, to experimental optical data. To ensure the accuracy of fitted parameters, we require that the corresponding dielectric function satisfies two sum rules,

$$\int_0^{\infty}\omega\varepsilon_2(0,\omega)\,\mathrm{d}\omega = \frac{\pi}{2}\sum_i A_i = \frac{\pi}{2}\omega_p^2 \tag{29}$$

$$\int_0^{\infty}\omega\,\mathrm{Im}\left(\frac{-1}{\varepsilon(0,\omega)}\right)\mathrm{d}\omega = \frac{\pi\omega_p^2}{2\varepsilon_b^2} \tag{30}$$

where ω_p would be the plasma energy of valence electrons if they were free.

2.3. Monte Carlo simulation

Elastic scatterings are simulated in the MC method by tracing electron trajectories. Data on electron path lengths between successive elastic collisions as well as polar and azimuthal scattering angles are recorded. The polar scattering angle, θ, after each collision is determined by the probability density function given by

$$P(\theta) = \frac{2\pi \sin\theta}{\sigma_t}\frac{\mathrm{d}\sigma}{\mathrm{d}\Omega} \tag{31}$$

where

$$\sigma_t = \int \frac{\mathrm{d}\sigma}{\mathrm{d}\Omega}\mathrm{d}\Omega \tag{32}$$

is the total elastic cross section. Assuming a Poisson distribution for elastic scattering events, the path length between two successive elastic collisions, s, is determined by [50]

$$P(s) = \frac{1}{\lambda_e}\exp\left(-\frac{s}{\lambda_e}\right). \tag{33}$$

Here the elastic mean free path of electrons is given by [51]

$$\lambda_e = (N\sigma_t)^{-1} \tag{34}$$

where N is the atomic density of the solid. The azimuthal scattering angle is determined by a uniform distribution due to the cylindrical symmetry of the scattering problem.

Simulations are repeated until either the electron leaves the sample or its total path length in the solid becomes so large that its contribution to the elastically backscattered intensity is negligible. The contribution from the jth electron to the elastically reflected current can be calculated from

$$\Delta I_j = \exp[-P_s(\alpha_{Ij}, E)]\exp[-P_s(\alpha_{Rj}, E)]\exp(-s_j/\lambda_i) \tag{35}$$

if the electron leaves the solid by an escape angle within the acceptance values and $\Delta I_j = 0$ otherwise, where s_j is the electron path length and α_{Ij} and α_{Rj} are, respectively, angles between the incident and reflected electron velocities and the surface normal. The factors $\exp[-P_s(\alpha_{Ij}, E)]$ and $\exp[-P_s(\alpha_{Rj}, E)]$ in equation (35) relate to the probabilities of incident and reflected electrons crossing the surface without surface excitations. The factor $\exp(-s_j/\lambda_i)$ represents the probability of an electron traversing the path length, s_j, in the solid without volume excitations. The elastic reflection coefficient can be calculated from

$$\eta_e = \frac{1}{m}\sum_{j=1}^{m}\Delta I_j \tag{36}$$

where m is the total number of generated trajectories.

3. Results and discussion

Figure 1 shows a plot of the static potential, $V_s(r)$, the exchange potential, $V_e(r)$, and the polarization potential, $V_p(r)$, for elastic scatterings of electrons as functions of the electron–atom distance in gold. Both the static potential and the exchange potential drop to zero at the Wigner–Seitz radius due to the vanishing electron density there.

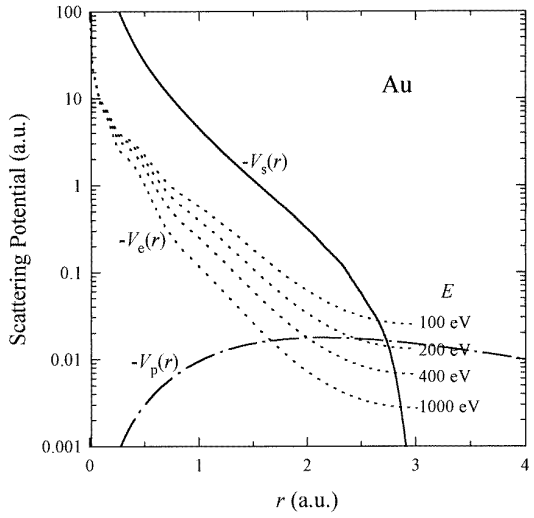

Figure 1. A plot of elastic scattering potentials as functions of the electron–atom distance in gold. Here V_s, V_e and V_p are, respectively, the static, exchange and polarization potentials. The exchange potential depends on the energy of electrons.

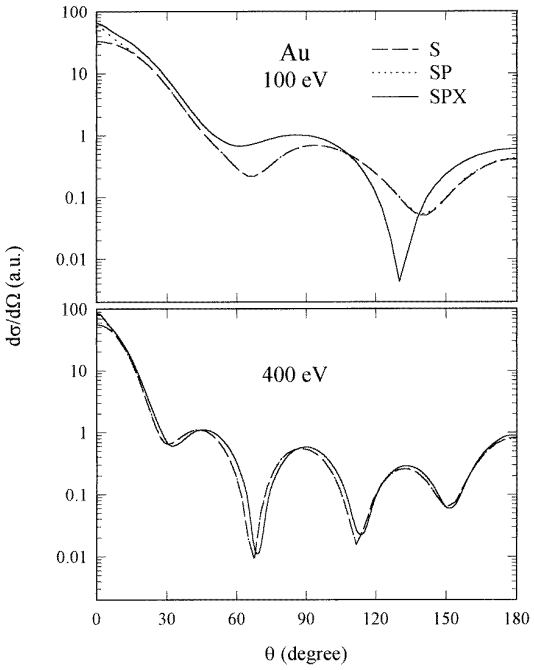

Figure 2. A comparison of elastic differential cross sections calculated using the S, SP and SPX scattering potentials as functions of the scattering angle, θ, for 100 and 400 eV electrons in gold.

The polarization potential, on the other hand, extends to a large distance, corresponding to a small scattering angle. Thus, the polarization potential is responsible for elastic scattering with small scattering angles. At small distances corresponding to large scattering angles, the exchange effect is more important than the polarization effect. The increase of exchange potential with decreasing electron

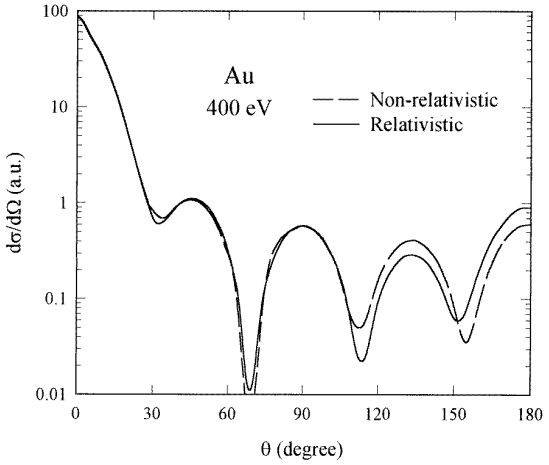

Figure 3. A comparison of elastic differential cross sections calculated using the relativistic and non-relativistic models as functions of the scattering angle, θ, for 400 eV electrons in gold.

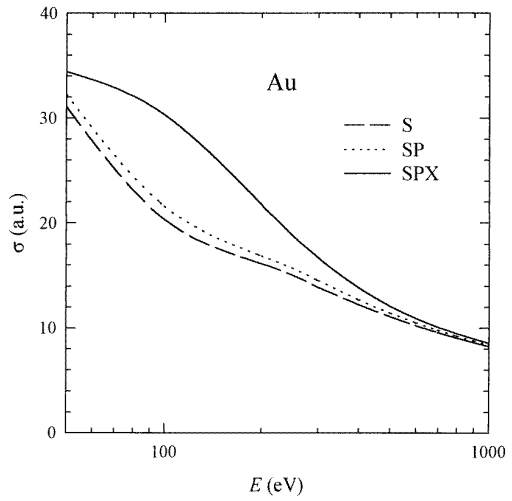

Figure 4. A comparison of elastic total cross sections calculated using the S, SP and SPX scattering potentials as functions of the electron energy in gold.

energy reveals that the exchange effect is significant for lower energy electrons.

Figure 2 shows a comparison of elastic differential cross sections calculated using the static (S), static and polarization (SP) and static, polarization and exchange (SPX) potentials for electrons of 100 and 400 eV in gold. As expected, the polarization potential makes a substantial contribution to the cross section only for predominately forwards scatterings, whereas, the exchange potential makes an important correction for backwards scatterings. This correction, however, is negligible for electron energies greater than about 400 eV. A comparison of elastic differential cross sections calculated using relativistic and non-relativistic models is made in figure 3 for 400 eV electrons in gold. It can be seen that the relativistic effect is important for backwards scatterings. The total elastic cross sections calculated using the S, SP and SPX

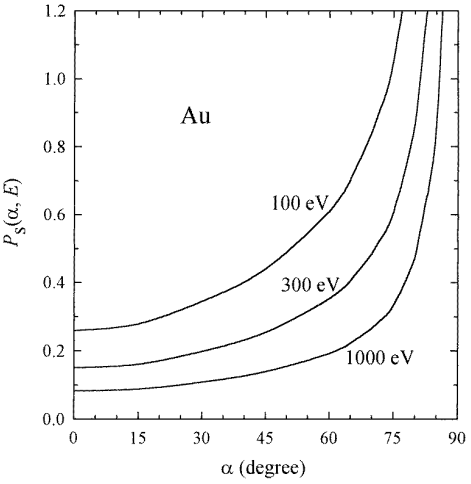

Figure 5. A plot of surface excitation probabilities in gold as a function of the electron incidence or escape angle, α, for several electron energies.

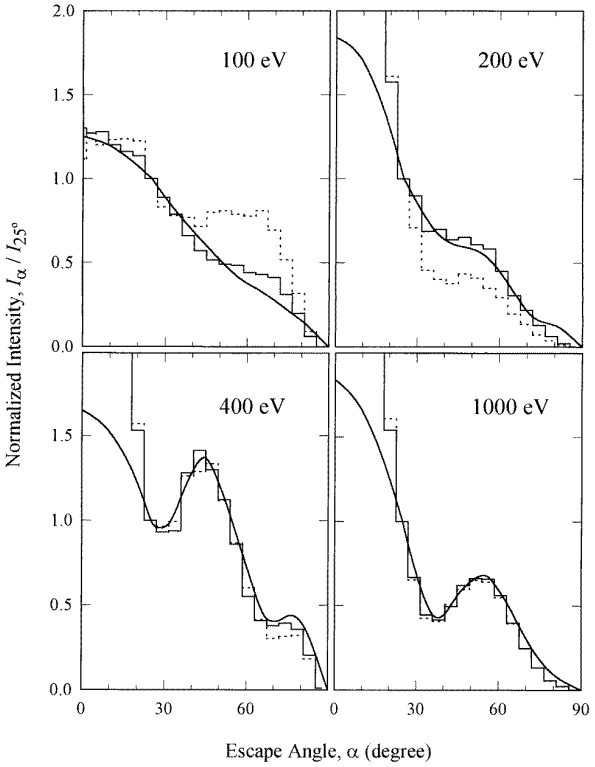

Figure 6. The angular distribution of electrons, with various energies, reflected elastically from gold surfaces. The full and dotted histograms are, respectively, MC results calculated using the SPX and S scattering potentials. The full curves are experimental data [19]. All results have been normalized with respect to the elastically reflected electron intensity at 25° escape angle.

potentials are plotted in figure 4 as functions of the electron energy in gold. It is observed that the polarization potential contributes slightly at all electron energies. The exchange potential, however, makes a significant contribution at electron energies below about 400 eV.

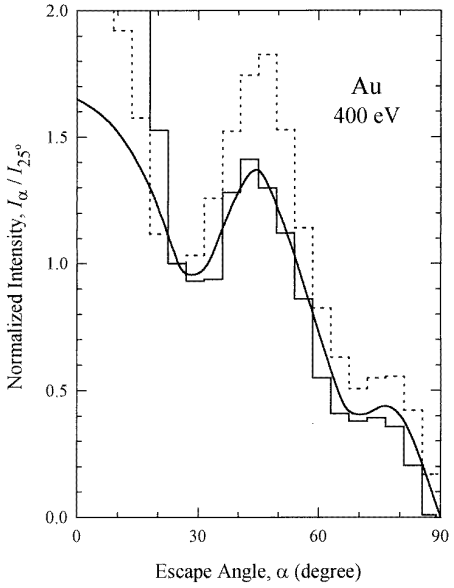

Figure 7. The angular distribution of 400 eV electrons reflected elastically from gold surfaces. The full and dotted histograms are, respectively, MC results calculated using the relativistic and non-relativistic models. The full curve shows experimental data [19]. All results have been normalized with respect to the elastically reflected electron intensity at 25° escape angle.

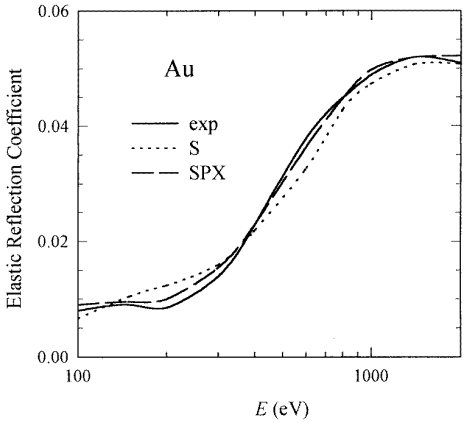

Figure 8. The elastic reflection coefficient of normally incident electrons reflected from gold surfaces into acceptance angles between 6° and 52° as a function of the electron energy. The broken and dotted curves are, respectively, calculated results using the SPX and S scattering potentials. The full curve shows experimental data [18].

Figure 5 is a plot of electron surface excitation probabilities in gold as a function of the cross angle (incidence or escape angle) between the electron velocity and the surface normal. The sharp increase in the SEP at large cross angles reveals that surface excitations are most probable for glancing electrons. This confirms the experimental observations [39]. Furthermore, the monotonic increase in the SEP with decreasing electron energy suggests that surface excitations are more important for lower energy electrons.

Figure 6 shows the angular distribution of electrons reflected elastically from gold surfaces. Note that all results correspond to normally incident electrons normalized with respect to the elastically backscattered electron intensity at 25° escape angle. The solid histograms are MC results of the present work using elastic differential cross sections calculated by the SPX approximation. For comparison, we plot experimental data (full curves) [19] and results computed using the S approximation for elastic differential cross sections (dotted histograms). Better agreement between experimental data and MC results was found by using the SPX approximation than was found by using the S approximation, especially for electron energies below 400 eV. A comparison of the angular distribution calculated using relativistic and non-relativistic elastic differential cross sections is made for 400 eV electrons reflected elastically from gold surfaces in figure 7. The agreement between experimental data and MC results obtained by using the relativistic model was better than that obtained by using the non-relativistic model for all escape angles.

Finally, we plot in figure 8 the elastic reflection coefficient computed using the S (dotted curve) and SPX (broken curve) approximations of the relativistic model for normally incident electrons reflected from gold surfaces into acceptance angles between 6° and 52°. Also plotted in figure 8 are experimental data (full curve) of Schmid *et al* [18]. Again, calculated results including polarization and exchange effects are in good agreement with experimental data at all electron energies.

4. Conclusions

MC calculations to study the influence of exchange, polarization and relativistic effects on the angular distribution and the elastic reflection coefficient for electrons backscattered from gold surfaces have been performed. These showed that the polarization effect made a contribution to elastic differential cross sections at small scattering angles, whereas the exchange and relativistic effects contributed to these cross sections at large scattering angles. These effects are important to the angular distribution and the elastic reflection coefficient for electron energies below 400 eV. MC results calculated in this work are in very good agreement with experimental data.

Acknowledgment

This research was supported by the National Science Council of the Republic of China under contract NSC86-2215-E-009-037.

References

[1] Kirschner J and Staib P 1973 *Phys. Lett.* **42** 335
[2] Kirschner J and Staib P 1975 *Appl. Phys.* **6** 99
[3] Pawley J B 1984 *J. Microsc.* **136** 45
[4] Joy D C 1985 *J. Microsc.* **140** 51
[5] Pawley J B 1990 *Scanning* **12** 247
[6] Joy D C 1991 *J. Microsc.* **161** 343
[7] Pawley J B 1992 *Advanced Electric Electron Physics* vol 83, ed P W Hawkes (New York: Academic) p 203

[8] Böngeler R, Golla U, Kässens M, Reimer L, Schindler B, Senkel R and Spranck M 1993 *Scanning* **15** 1
[9] Gergely G 1981 *Surf. Interface Anal.* **3** 201
[10] Gergely G 1983 *Vacuum* **33** 89
[11] Jablonski A 1985 *Surf. Sci.* **151** 166
[12] Gergely G 1986 *Scanning* **8** 203
[13] Gruzza B, Achad B and Pariset C 1986 *J. Phys. D: Appl. Phys.* **19** 137
[14] Donlinski W, Mróz S and Zagórski M 1988 *Surf. Sci.* **200** 361
[15] Lesiak B, Jablonski A, Prussak Z and Mrozek P 1989 *Surf. Sci.* **223** 213
[16] Gruzza B and Pariset C 1991 *Surf. Sci.* **247** 408
[17] Jardin C, Gergely G and Gruzza B 1992 *Surf. Interface Anal.* **19** 5
[18] Schmid R, Gaukler K B and Seiler B 1983 *Scanning Electron Microscopy* vol II, ed O Johari (Chicago: IIT Research Institute) p 501
[19] Bronshtein I M and Pronin V P 1975 *Fiz. Tverd. Tela* **17** 2086 (Engl. Transl.1976 *Sov. Phys. Solid State* **17** 1363)
[20] Jablonski A, Gryko J, Kraaer J and Touggard S 1989 *Phys. Rev.* B **39** 61
[21] Jablonski A 1991 *Phys. Rev.* B **43** 7546
[22] Jablonski A, Hansen H S, Jansson C and Touggard S 1992 *Phys. Rev.* B **45** 3694
[23] Jablonski A, Jasson C and Touggard S 1993 *Phys. Rev.* B **47** 7420
[24] Bonham R A and Strand T G 1963 *J. Chem. Phys.* **39** 2200
[25] Tucker T C, Roberts L D, Nestor C W and Carson T A 1969 *Phys. Rev.* **178** 998
[26] Raether H 1980 *Excitations of Plasmons and Interband Transitions by Electrons* (New York: Springer)
[27] Ritchie R H and Howie A 1977 *Phil. Mag.* **36** 463
[28] Kwei C M, Chen Y F, Tung C J and Wang J P 1993 *Surf. Sci.* **293** 202
[29] Mott N F and Massey H S W 1987 *Theory of Atomic Collisions* 3rd edn (Oxford: Oxford University Press)
[30] Mittleman M H and Watson M K 1960 *Ann. Phys., Lpz.* **10** 268
[31] Riley M E and Truhlar D G 1975 *J. Chem. Phys.* **63** 2182
[32] Jhanwar B L and Khare S P 1976 *J. Phys. B: At. Mol. Phys.* **9** L527
[33] Joshipura K N 1986 *Solid State Commun.* **60** 277
[34] Joshipura K N and Mohanan S 1988 *Int. J. Mod. Phys.* B **2** 461
[35] Öztürk N, Williamson W Jr and Antolak A J 1991 *J. Appl. Phys.* **70** 537
[36] Rehr J J, Zaremba E and Kohn W 1975 *Phys. Rev.* B **12** 2062
[37] Mott N F 1929 *Proc. R. Soc.* A **124** 425
[38] Tung C J and Ritchie R H 1977 *Phys. Rev.* B **16** 4302
[39] Egerton R F 1986 *Electron Energy-Loss Spectroscopy in the Electron Microscope* (New York: Plenum)
[40] Ritchie R H 1957 *Phys. Rev.* **106** 874
[41] Tung C J, Chen Y F, Kwei C M and Chou T L 1994 *Phys. Rev.* B **49** 16 684
[42] Kunz C 1964 *Z. Phys.* **180** 127
[43] Creuzburg M 1963 *Z. Phys.* **174** 511
[44] Pettit R B, Silicox J and Vincent R 1975 *Phys. Rev.* B **11** 3116
[45] Lucas A A 1971 *Phys. Rev. Lett.* **26** 229
[46] Evans E and Mills D L 1972 *Phys. Rev.* B **5** 4126
[47] Evans E and Mills D L 1973 *Phys. Rev.* B **7** 853
[48] Schilling J 1976 *Z. Phys.* B **25** 61
[49] Smith D Y and Shiles E 1978 *Phys. Rev.* B **17** 4689
[50] Reimer L 1985 *Scanning Electron Microscopy* (New York: Springer) p 114
[51] Schimizu R, Kataoka Y, Ikuta T, Koshikawa T and Hashimoto H 1976 *J. Phys. D: Appl. Phys.* **9** 101